

Parameter Estimation Solving a Weak Constraint Variational Formulation for an Ekman Model

Mette Eknes and Geir Evensen

Nansen Environmental and Remote Sensing Center, Bergen, Norway

Abstract

A weak constraint variational formulation is used for inverse calculations and parameter estimation in a one-dimensional Ekman model. When parameters in the model are allowed to contain errors the inverse problem becomes nonlinear even if the model itself is linear. It is shown that a convergent iteration can be defined for the nonlinear system of Euler–Lagrange equations and that improved estimates of the poorly known parameters can be calculated by solving the inverse problem for each of the linear iterates using the representer method. The formulation of the variational problem and the solution methods are illustrated using a simple example. The use of a simple dynamical model makes it possible to give an instructive presentation of the representer method. The method is finally used in an example using real current meter data. It is shown that the weak constraint formulation results in smooth solutions in good agreement with the data all through the water column, and that it is superior to the traditional strong constraint inverse estimate.

Introduction

Data assimilation and inverse methods are normally used for generating estimates of dynamical variables, taking into account both the information about the dynamics from a dynamical model, and the information about the true state which is contained in a set of measurements. Such techniques have also been proposed as a tool for parameter estimation in dynamical models, although only a few works have so far considered the parameter estimation problem in this context. Examples are *Smedstad and O'Brien* [1991] who estimated the phase speeds in a reduced-gravity model of equatorial waves, using a strong constraint variational formulation, and *Yu and O'Brien* [1991, 1992], who used a modified one-dimensional Ekman-layer model in combination with variational optimal control techniques to simultaneously estimate the surface wind-drag coefficient and the vertical profile of the eddy viscosity from observed data.

In *Yu and O'Brien* [1991] a cost function was defined where the first guesses of the diffusion coefficient and the wind-drag coefficient was penalized in addition to the residual between the model-results and the observations. However, there was no penalty on the first guess initial conditions. Without such a penalty, every choice of initial conditions can be used, and there may exist many initial conditions resulting in a solution which interpolates the data and give a penalty function equal to zero [Bennett and Miller, 1990]. In *Yu and O'Brien* [1992] such a term was included, although the resulting equation for the initial condition was incorrect. The cost function was minimized using the adjoint technique to calculate the gradient of the penalty function with respect to the control parameters, i.e., the initial condition, the wind-drag and the eddy viscosity with the dynamical model acting as a strong constraint.

Here, the parameter estimation problem is re-examined using a weak constraint variational inverse formulation. Thus, the model, the initial and boundary conditions, the measurements, the diffusion parameter and the wind-drag coefficient are all allowed to contain errors. The strong constraint inverse may be obtained as a limiting case where the model errors approach zero.

If the wind-drag C_d and the vertical diffusion parameter A are considered known, the inverse formulation for the Ekman-model is linear. However, allowing them to contain errors, the problem becomes nonlinear and some sort of iteration procedure must be used to solve the Euler–Lagrange equations. Here, it is shown that by defining an iteration for the unknown parameters, each of the linear iterates for the Euler–Lagrange equations can be solved exactly using the representer method [Bennett, 1992]. Such an approach is similar to previous applications of the representer method with nonlinear dynamics. For instance, *Bennett and Thorburn* [1992], and *Bennett et al.* [1993], solved for the weak constraint inverse of a nonlinear barotropic quasi-

geostrophic model by defining a convergent sequence of linear iterates of the Euler–Lagrange equations, where each iterate could be solved using the representer technique.

In the next section, the inverse formulation is discussed and the Euler–Lagrange equations are derived. Then, in Section 3, the representer method is applied to decouple the Euler–Lagrange equations for the linear problem resulting when the diffusion parameter and the wind drag coefficient are assumed known. In Section 4, the iterations of the Euler–Lagrange equations used to solve for the diffusion parameter and the wind-drag coefficient are defined, and in Section 5, an example that illustrates the method is presented. Finally, the LOTUS-3 data [Tarbell et al., 1984; Bowers et al., 1986] has been used in a real data assimilation experiment to compare the results of a weak constraint formulation with the results of *Yu and O'Brien* [1991, 1992].

Inverse Formulation

The Ekman model can be written in nondimensional form by defining characteristic scales for the dependent and independent variables. The time scale is $\tau = f^{-1}$, where f is the Coriolis parameter, and the depth scale is the Ekman layer thickness $\delta_e = \sqrt{2A(0)f^{-1}}$, where $A(0)$ is the diffusion coefficient at the surface. A velocity scale becomes $\delta_e \tau^{-1} = \sqrt{2A(0)f}$, and the diffusion coefficient is scaled by $2A(0)$. The atmospheric wind speed is scaled by $\sqrt{2A(0)f\rho_w\rho_a^{-1}}$ where ρ_a and ρ_w are the air- and water-densities. The nondimensional Ekman layer model then becomes

$$\frac{\partial \mathbf{u}}{\partial t} + \mathbf{k} \times \mathbf{u} = \frac{\partial}{\partial z} \left(A \frac{\partial \mathbf{u}}{\partial z} \right) + \mathbf{q}, \quad (1)$$

where $\mathbf{u}(z, t)$ is the horizontal velocity vector, $A = A(z)$ is the diffusion coefficient and $\mathbf{q}(z, t)$ is the unknown model error. The initial conditions are given as

$$\mathbf{u}(z, 0) = \mathbf{U}_0 + \mathbf{a}, \quad (2)$$

where \mathbf{a} contains the errors in the first guess initial condition \mathbf{U}_0 . The boundary conditions for the model are

$$A \frac{\partial \mathbf{u}}{\partial z} \Big|_{z=0} = \left(C_d \sqrt{u_a^2 + v_a^2} \right) \mathbf{u}_a + \mathbf{b}_0, \quad (3)$$

$$A \frac{\partial \mathbf{u}}{\partial z} \Big|_{z=-H} = \mathbf{o} + \mathbf{b}_H, \quad (4)$$

where the position $z = 0$ is at the ocean surface and the lower boundary is at $z = -H$, C_d is the wind-drag coefficient, \mathbf{u}_a is the atmospheric wind-speed, and \mathbf{b}_0 and \mathbf{b}_H are the unknown errors in the boundary conditions.

Now a set of measurements, \mathbf{d} , of the true solution are assumed given and linearly related to the model variables by the measurement equation

$$\mathbf{d} = \mathcal{L}[\mathbf{u}^t] + \epsilon. \quad (5)$$

Here, \mathcal{L} is a vector of linear measurement functionals, \mathbf{u}^t is the true state, and $\boldsymbol{\epsilon}$ is the measurement errors.

If all the error-terms are zero, the problem becomes over-determined and no solution can be found in general. However, by allowing the model dynamics, the initial- and boundary conditions, and the measurements to contain errors, a solution can be found which minimizes these error terms in a weighted least squares sense.

Here we also allow for the first guesses of the wind-drag and the diffusion coefficient, C_{d_0} and $A_0(z)$, to contain errors, i.e.,

$$C_d = C_{d_0} + p_{C_d}, \quad (6)$$

$$A(z) = A_0(z) + p_A(z), \quad (7)$$

where p_{C_d} and $p_A(z)$ are the unknown error terms. Thus, a combined inverse and parameter estimation problem is formulated. All the error terms are assumed to be normal distributed with zero mean and known covariances.

A convenient variational formulation is

$$\begin{aligned} \mathcal{J}[\mathbf{u}, C_d, A] &= \int_0^T dt_1 \int_0^T dt_2 \int_{-H}^0 dz_1 \int_{-H}^0 dz_2 \\ &\quad \mathbf{q}^T(z_1, t_1) \mathbf{W}_{qq}(z_1, t_1, z_2, t_2) \mathbf{q}(z_2, t_2) \\ &+ \int_{-H}^0 dz_1 \int_{-H}^0 dz_2 \mathbf{a}^T(z_1) \mathbf{W}_{aa}(z_1, z_2) \mathbf{a}(z_2) \\ &+ \int_0^T dt_1 \int_0^T dt_2 \mathbf{b}_0^T(t_1) \mathbf{W}_{b_0 b_0}(t_1, t_2) \mathbf{b}_0(t_2) \quad (8) \\ &+ \int_0^T dt_1 \int_0^T dt_2 \mathbf{b}_H^T(t_1) \mathbf{W}_{b_H b_H}(t_1, t_2) \mathbf{b}_H(t_2) \\ &+ \int_{-H}^0 dz_1 \int_{-H}^0 dz_2 p_A(z_1) W_{AA}(z_1, z_2) p_A(z_2) \\ &+ p_{C_d} W_{C_d C_d} p_{C_d} \\ &+ \boldsymbol{\epsilon}^T \mathbf{w} \boldsymbol{\epsilon}. \end{aligned}$$

A simpler way of writing this may be

$$\begin{aligned} \mathcal{J}[\mathbf{u}, C_d, A] &= \mathbf{q}^T \bullet \mathbf{W}_{qq} \bullet \mathbf{q} + \mathbf{a}^T \circ \mathbf{W}_{aa} \circ \mathbf{a} \\ &+ \mathbf{b}_0^T * \mathbf{W}_{b_0 b_0} * \mathbf{b}_0 + \mathbf{b}_H^T * \mathbf{W}_{b_H b_H} * \mathbf{b}_H \quad (9) \\ &+ p_A \circ W_{AA} \circ p_A + p_{C_d} W_{C_d C_d} p_{C_d} + \boldsymbol{\epsilon}^T \mathbf{w} \boldsymbol{\epsilon}, \end{aligned}$$

where \bullet means integration both in space and time, \circ means integration in space and $*$ means integration in time.

The weights $\mathbf{W}_{??}$, are functional inverses of the respective covariances $\mathbf{Q}_{??}$, e.g., for the model weight,

$$\mathbf{Q}_{qq} \bullet \mathbf{W}_{qq} = \delta(z_1 - z_3) \delta(t_1 - t_3) \mathbf{I}, \text{ or written out,}$$

$$\begin{aligned} &\int_0^T dt_2 \int_{-H}^0 dz_2 \mathbf{Q}_{qq}(z_1, t_1, z_2, t_2) \mathbf{W}_{qq}(z_2, t_2, z_3, t_3) \\ &= \delta(z_1 - z_3) \delta(t_1 - t_3) \mathbf{I}, \end{aligned} \quad (10)$$

\mathbf{w} is the inverse of the measurement error covariance matrix \mathbf{w}^{-1} and the weight $W_{C_d C_d}$ is one over the error variance of p_{C_d} . These weights determine the spatial and temporal scales for the physical problem and ensure smooth influences from the measurements. Note that the first guesses of all unknown quantities are penalized. This is required to ensure a unique solution of the inverse as shown by *Bennett and Miller* [1990]. Even if no measurements are available, the inverse will still have a unique solution corresponding to the first guess solution. This implies that the role of each of the measurements is to add a specific contribution (influence function) to the first guess solution.

Note that other estimators than least squares could be defined. However, the least-squares formulation is attractive for several reasons. If the unknown errors are Gaussian, i.e., completely explained by the two first statistical moments, mean and covariance, then minimizing (8) is equivalent to finding the maximum likelihood estimate. When working with methods that involve the Euler-Lagrange equations these are readily derived and the derivatives of the penalty function exist everywhere.

Some important differences between the formulation used in this paper and the previous works by *Yu and O'Brien* [1991, 1992], should be mentioned. Here, in addition to allowing the model and boundary conditions to contain errors, nondiagonal weights have been used in the penalty function (8) to ensure smooth results. In *Yu and O'Brien* [1991, 1992] the weights were diagonal which means that there was no regularization imposed on the control variables, i.e., they would accept noisy estimates as solutions.

By substituting for the error terms from equations (1-7) in the penalty function $\mathcal{J}[\mathbf{u}, C_d, A]$ and taking the variation with respect to \mathbf{u} , the system of Euler-Lagrange equations becomes

$$\frac{\partial \mathbf{u}}{\partial t} + \mathbf{k} \times \mathbf{u} = \frac{\partial}{\partial z} \left(A \frac{\partial \mathbf{u}}{\partial z} \right) + \mathbf{Q}_{qq} \bullet \boldsymbol{\lambda}, \quad (11)$$

with initial conditions

$$\mathbf{u}|_{t=0} = \mathbf{U}_0 + \mathbf{Q}_{aa} \circ \boldsymbol{\lambda}, \quad (12)$$

and boundary conditions

$$A \frac{\partial \mathbf{u}}{\partial z} \Big|_{z=0} = C_d \sqrt{u_a^2 + v_a^2} \mathbf{u}_a + \mathbf{Q}_{b_0 b_0} * \boldsymbol{\lambda}, \quad (13)$$

$$A \frac{\partial \mathbf{u}}{\partial z} \Big|_{z=-H} = -\mathbf{Q}_{b_H b_H} * \boldsymbol{\lambda}. \quad (14)$$

The so-called adjoint equation becomes

$$-\frac{\partial \boldsymbol{\lambda}}{\partial t} - \mathbf{k} \times \boldsymbol{\lambda} = \frac{\partial}{\partial z} \left(A \frac{\partial \boldsymbol{\lambda}}{\partial z} \right) + \mathcal{L}^T[\delta(z - z_2)\delta(t - t_2)]\mathbf{w}(\mathbf{d} - \mathcal{L}[\mathbf{u}]), \quad (15)$$

subject to the “final” conditions

$$\boldsymbol{\lambda}|_{t=T} = \mathbf{o}, \quad (16)$$

and the boundary conditions

$$\left. \frac{\partial \boldsymbol{\lambda}}{\partial z} \right|_{z=0, z=-H} = \mathbf{o}. \quad (17)$$

The system (11–17) are the Euler-Lagrange equations which here comprise a two-point boundary value problem in space and time, and since they are coupled, they must be solved simultaneously. Equation (11) is the dynamical model forced by a term that estimates the model errors and contains the adjoint variable. A similar coupling to the adjoint variable is also contained in the initial conditions (12) and boundary conditions (13) and (14). The “backward” or adjoint equation (15), which strictly speaking is the Euler Lagrange equation, contains a weak coupling to the “forward” variable \mathbf{u} at measurement locations. Note that the strong constraint assumption removes the coupling of equation (11) to the adjoint variables, but the Euler-Lagrange equations are still coupled through the initial- and boundary-conditions (12–14). In the adjoint technique this coupling is iterated using a gradient descent procedure.

Since the drag coefficient and the diffusion are allowed to contain errors, the variation of the penalty function with respect to these parameters must also be taken. This results in the additional equations

$$C_d = C_{d_0} + Q_{C_d C_d} \int_0^T \boldsymbol{\lambda}^T(0, t) \mathbf{u}_a dt, \quad (18)$$

$$A = A_0 - Q_{AA} \bullet \frac{\partial \boldsymbol{\lambda}^T}{\partial z} \frac{\partial \mathbf{u}}{\partial z}, \quad (19)$$

for the wind-drag coefficient and the diffusion parameter. The addition of the two equations (18) and (19) makes the system of Euler–Lagrange equations nonlinear.

Representer Solution

The nonlinearity appearing in the Euler-Lagrange equations for parameter estimation problems suggests that some kind of iterative procedure should be used. If the parameters A and C_d are given, the remaining Euler–Lagrange equations are linear and can be solved exactly using a representer expansion. It is therefore proposed to iterate the equations (18) and (19) and to solve for each of the linear iterates using the representer method.

Assume now that the forward and backward variables can be expressed as

$$\mathbf{u} = \mathbf{u}_F + \sum_{m=1}^M b_m \mathbf{r}_m, \quad (20)$$

$$\boldsymbol{\lambda} = \boldsymbol{\lambda}_F + \sum_{m=1}^M b_m \boldsymbol{\alpha}_m. \quad (21)$$

The coefficients b_m are amplitudes for the M influence functions or representer, $\mathbf{r}_m(z, t)$, of which there are one for each of the measurements. Here, the forward variable contains both a u - and a v -component, and so will each of the representer.

If the expressions (20) and (21) are substituted into the Euler-Lagrange equations, one first observe that the first guess solution $\boldsymbol{\lambda}_F = \mathbf{o}$, is the solution of the homogeneous backward model, while \mathbf{u}_F is a first guess model solution with $\boldsymbol{\lambda}_F = \mathbf{o}$, i.e., the model solution found when no information from the measurements are used.

The M representer are found by solving the initial value problems

$$\frac{\partial \mathbf{r}_m}{\partial t} + \mathbf{k} \times \mathbf{r}_m = \frac{\partial}{\partial z} \left(A \frac{\partial \mathbf{r}_m}{\partial z} \right) + \mathbf{Q}_{qq} \bullet \boldsymbol{\alpha}_m, \quad (22)$$

with initial conditions

$$\mathbf{r}_m|_{t=0} = \mathbf{Q}_{aa} \circ \boldsymbol{\alpha}_m, \quad (23)$$

and boundary conditions

$$A \frac{\partial \mathbf{r}_m}{\partial z} \Big|_{z=0} = \mathbf{Q}_{b_0 b_0} * \boldsymbol{\alpha}_m, \quad (24)$$

$$A \frac{\partial \mathbf{r}_m}{\partial z} \Big|_{z=-H} = -\mathbf{Q}_{b_H b_H} * \boldsymbol{\alpha}_m. \quad (25)$$

These equations are coupled to the adjoints of the representer, $\boldsymbol{\alpha}_m$, which satisfy the “final” value problems

$$-\frac{\partial \boldsymbol{\alpha}_m}{\partial t} - \mathbf{k} \times \boldsymbol{\alpha}_m = \frac{\partial}{\partial z} \left(A \frac{\partial \boldsymbol{\alpha}_m}{\partial z} \right) + \mathcal{L}_m[\delta(z - z_2)\delta(t - t_2)], \quad (26)$$

with “final” conditions

$$\boldsymbol{\alpha}_m|_{t=T} = \mathbf{o}, \quad (27)$$

and boundary conditions

$$\left. \frac{\partial \boldsymbol{\alpha}_m}{\partial z} \right|_{z=0, z=-H} = \mathbf{o}. \quad (28)$$

The equations for the representer and their adjoints are now decoupled since the dependence to the forward variable has been removed in equation (26). This has been done by choosing \mathbf{b} to satisfy the linear system

$$(\mathbf{R} + \mathbf{w}^{-1})\mathbf{b} = \mathbf{d} - \mathcal{L}[\mathbf{u}_F], \quad (29)$$

where the representer matrix \mathbf{R} is defined as

$$\mathbf{R}(:, m) = \mathcal{L}[\mathbf{r}_m], \quad (30)$$

i.e., \mathbf{R} is constructed by measuring the representer. By rearranging equation (29), one can write

$$\mathbf{b} = \mathbf{w}(\mathbf{d} - \mathcal{L}[\mathbf{u}_F + \sum_{m=1}^M b_m \mathbf{r}_m]) = \mathbf{w}(\mathbf{d} - \mathcal{L}[\mathbf{u}]). \quad (31)$$

This expression can be used on the right hand side of (15) to decouple the Euler–Lagrange equations.

The solution procedure for the representer method can be summarized as follows. First, each of the representer is calculated by a backward integration of (26–28) to get α_m followed by a forward integration of (22–25) to get \mathbf{r}_m . Note that only the representer matrix is required to find \mathbf{b} , so only the “measurements” of the representer need to be stored. The calculations of the M representer are entirely independent of each other and may therefore be computed very efficiently on a multi-processor computer [Bennett and Baugh, 1992]. When the representer matrix has been generated, the system (29) can be solved after a forward integration for \mathbf{u}_F to calculate the residual between the measurements and the first guess solution appearing on the right hand side of (29). The coefficient vector \mathbf{b} is then used in equation (15) to find λ by a backward integration of (15–17) followed by a forward integration of (11–14) to find the inverse solution. The total cost of the solution algorithm is the integration of $2M + 3$ initial value problems, and only one field as function of (z, t) needs to be stored simultaneously.

It should be noted that the expression (20) for \mathbf{u} , does not represent all arbitrary functions of x and t . However, all observable fields can be represented by (20) and only the unobservable fields have been rejected [see Bennett, 1992]. Thus, the problem has been reduced to searching for the solution in an M -dimensional space spanned by the representer.

A posterior error covariance estimate can be calculated for the solution by using

$$\begin{aligned} \mathbf{C}\mathbf{u}\mathbf{u}(z_1, t_1, z_2, t_2) &= \mathbf{F}(z_1, t_1, z_2, t_2) \\ &\quad - \mathbf{r}(z_1, t_1)^T (\mathbf{R} + \mathbf{w}^{-1})^{-1} \mathbf{r}(z_2, t_2), \end{aligned} \quad (32)$$

where $\mathbf{F}(z_1, t_1, z_2, t_2)$ is the representer or prior space-time covariance function for the first guess solution, and $\mathbf{r}^T (\mathbf{R} + \mathbf{w}^{-1})^{-1} \mathbf{r}$ is the explained error covariance. Normally, only the variances are needed and $\mathbf{F}(z, t, z, t)$ may be estimated using statistical simulations. It should also be mentioned that each of the representer can be expressed as

$$\mathbf{r}_m = \mathcal{L}_m[\mathbf{f}], \quad (33)$$

thus, the representer method is equivalent to Gauss–Markov smoothing in space and time [Bennett, 1992]. A comparison of the representer method and the Kalman filter has been given in Evensen [1994a].

Parameter Estimation

In the previous section it was illustrated how the Euler–Lagrange equations for the weak constraint inverse formulation could be solved exactly when $A(z)$ and C_d were known. When the parameters are allowed to contain errors, the inverse problem becomes nonlinear and therefore an iteration will be used for the equations (18) and (19) for $A(z)$ and C_d . In each iteration, the representer technique will be used to solve for the corresponding inverse estimate.

The equations (18) and (19) were here iterated using a gradient descent method, i.e.,

$$\begin{aligned} C_d^{n+1} &= C_d^n - \\ &\gamma \left(C_d^n - C_{d_0} - Q_{C_d C_d} \int_0^T \lambda_n^T \sqrt{u_a^2 + v_a^2} \mathbf{u}_a dt \right), \end{aligned} \quad (34)$$

$$A^{n+1}(z) = A^n(z) -$$

$$\beta \left(A^n(z) - A_0(z) + Q_{pp} \bullet \frac{\partial \mathbf{u}_n^T}{\partial z} \frac{\partial \lambda_n}{\partial z} \right), \quad (35)$$

where γ and β are properly chosen constants. These equations are now iterated to generate new guesses C_d^{n+1} and A^{n+1} , which are used to solve for \mathbf{u}_{n+1} and λ_{n+1} using the representer technique described in the previous section. Other iteration techniques were also examined and gave satisfactory convergence.

As pointed out in Bennett [1992], Yu and O’Brien [1991] did not impose a smoothing constraint on the diffusion coefficient $A(z)$. It was therefore not clear if there was any difference in varying $A(0)$ or C_d in the surface condition (13), since $A(z)$ may be discontinuous. However, here the nondiagonal weights will ensure a smooth $A(z)$. It is therefore expected that a vertical profile of the solution for \mathbf{u} , which is consistent with the measurements, will determine the profile for $A(z)$, while C_d will adjust to provide the correct surface forcing. Here we also included an error term in the actual boundary condition to account for errors in the atmospheric wind data. Clearly, these error sources give rise to a highly nonlinear problem, where multiple minima may exist and a unique solution is not guaranteed.

Example

Here a simple example will be used to illustrate the method which is proposed for parameter estimation. A constant wind with $\mathbf{u}_a = (10 \text{ m s}^{-1}, 10 \text{ m s}^{-1})$ has been used to spin up the vertical velocity structure in the first guess solution, starting with an initial condition $\mathbf{u}(z, 0) = \mathbf{0}$ and then performing 50 hours of integration. The reference case, from which velocity data are extracted, is generated by continuing the integration for another 50 hours. Values for some of the physical parameters are given in Table 1. Note that the values for variables in the text and the tables are all given in dimensional units.

By measuring the reference case and adding Gaussian noise, eight simulated measurements of \mathbf{u} were generated, i.e., a total of 16 measurements of u - and v -components were used. The locations of the measurements are shown in the figures below.

All error terms are assumed to be unbiased and the error covariances were specified as follows:

$$\mathbf{Q}_{aa}(z_1, z_2) = \sigma_a^2 \exp \left\{ - \left(\frac{z_1 - z_2}{l_a} \right)^2 \right\} \mathbf{I}, \quad (36)$$

$$\mathbf{Q}_{b_0 b_0}(t_1, t_2) = \sigma_{b_0}^2 \delta(t_1 - t_2) \mathbf{I}, \quad (37)$$

$$\mathbf{Q}_{b_H b_H}(t_1, t_2) = \sigma_{b_H}^2 \delta(t_1 - t_2) \mathbf{I}, \quad (38)$$

$$\mathbf{Q}_{qq}(z_1, t_1, z_2, t_2) = \sigma_q^2 \exp \left\{ - \left(\frac{z_1 - z_2}{l_q} \right)^2 \right\} \delta(t_1 - t_2) \mathbf{I}, \quad (39)$$

$$\mathbf{Q}_{AA}(z_1, z_2) = \sigma_A^2 \exp \left\{ - \left(\frac{z_1 - z_2}{l_A} \right)^2 \right\}, \quad (40)$$

$$\mathbf{Q}_{C_d C_d} = \sigma_{C_d}^2, \quad (41)$$

$$\mathbf{w}^{-1} = \sigma_o^2 \mathbf{I}. \quad (42)$$

Here, it has been assumed that the model and the boundary errors are uncorrelated in time. This is convenient for computational reasons, but for more realistic applications such a correlation should probably be included. Values for the variances and the de-correlation lengths are given in Table 2.

To illustrate the solution procedure using the representer method in more detail, the variables α_5 , \mathbf{r}_5 , and λ and the right hand sides, $\mathbf{Q}_{qq} \bullet \alpha_5$ and $\mathbf{Q}_{qq} \bullet \lambda$, are given in Figure 2 with u - and v -components in the left and the right column, respectively. These plots demonstrate how the information from the measurements are taken into account and influence the solution. Measurement number five corresponds to the u -component at the location $(Z_5, T_5) = (-20.0, 25.0)$.

The upper row shows the components of α_5 , and it is clear from equation (26) that the u -component of α_5 is forced by the δ -function at the measurement location. This information is then propagated backward in time, while the u - and v -components interact during the integration.

The α_m 's are then used on the right hand side of the forward equation for the representer and also in the initial and boundary conditions. The convolution $\mathbf{Q}_{qq} \bullet \alpha_5$ tends to smooth the α_5 -field according to the covariance functions contained in \mathbf{Q}_{qq} , as can be observed from the second row in Figure 2.

The representer \mathbf{r}_5 is smooth and is oscillating in time with a period reflecting the inertial oscillations described by the dynamical model. Note that the representers will have a discontinuous time derivative at the measurement location since the right hand side $\mathbf{Q}_{qq} \bullet \alpha_5$ is discontinuous there. However, if a correlation in time

was allowed in \mathbf{Q}_{qq} , then $\mathbf{Q}_{qq} \bullet \alpha_5$ would be continuous and the representer \mathbf{r}_5 , would be smooth.

After all the representers have been calculated and measured to generate the representer matrix, the coefficient \mathbf{b} is calculated and used in equation (15) to decouple the Euler–Lagrange equations. The u - and v -components of λ (Figure 2) illustrates how the various measurements have a different impact determined by values of the coefficients in \mathbf{b} , which again are determined by the quality of the first guess solution versus the quality of the measurements and the residual between the measurements and the first guess solution. After λ is found the right-hand side in the forward model equation can be constructed through the convolution $\mathbf{Q}_{qq} \bullet \lambda$, and this field is given at the bottom of Figure 2. Clearly, the role of this term is to force the solution to smooth the measurements.

The first guess, the reference solution, and the inverse estimate are given in Figure 1. The reference solution is regenerated quite well, even though the first guess solution is out of phase with the reference case, and the measurements does not resolve the time period of the oscillation. In fact, a single measurement may suffice for reconstructing the correct phase since the corresponding representer will carry the information both forward and backward in time, although the errors will be larger with less measurements.

The estimation of the diffusion parameter $A(z)$ is illustrated in Figure 3, where the first guess $A_0(z)$ and the reference $A(z)$, are shown together with the estimate $\hat{A}(z)$. The weak signal below the Ekman layer makes it difficult to correct an erroneous first guess of the diffusion parameter in the deep ocean. Note also that the estimate for A does not coincide with the reference diffusion parameter but is located somewhere in between the first guess A_0 and the exact A at most of the depths. Some places, however the estimate is located to the left of both the first guess and the reference diffusion. The reason for this is the nonlinearity of the problem, and thus a nonconvex penalty function.

The estimation of the the wind drag coefficient C_d is shown in Figure 4, and the estimate is a value somewhere in between the first guess and the reference value. It should at this time be commented on the fact that the estimated values for the unknown parameters found in *Yu and O'Brien* [1991, 1992] did not show any effect from the penalty of the first guess values. This indicates that zero weights were used for the first guesses. What they actually did was to replace the first guess value with the current estimate in each iteration. A different variational problem was therefore implicitly assumed in each iteration, and they had in reality no penalty on the first guess estimates. They therefore allowed for every arbitrary and nonsmooth function to be a solution for $A(z)$. Unless there is enough independent information contained in the measurements to close this problem, many solutions may be found which interpolates the measurements and give the value zero to the penalty

functions.

Assimilation of LOTUS-3 time series

The representer implementation will now be examined using the LOTUS-3 data set [Bowers *et al.*, 1986] in a similar setup to the one used by Yu and O'Brien [1991, 1992]. The LOTUS-3 measurements were collected in the northwestern Sargasso Sea (34° N, 70° W) during the summer of 1982. Current meters fixed at depths 5, 10, 15, 20, 25, 35, 50, 65, 75 and 100 meters measured the *in situ* currents, and a wind recorder mounted on top of the LOTUS-3 tower measured the wind speeds. The sampling interval was 15 minutes and the data used by Yu and O'Brien [1991, 1992] were collected in the period from the 30th of June to the 9th of July 1982. Here data from the same time period are used. However, while Yu and O'Brien [1991, 1992] used every data collected during the 10 days, we have used a subsampled data set consisting of measurements collected at a 5 hour time interval at the depths 5, 25, 35, 50, and 75 meters. The reason for not using all the measurements is to reduce the size of the representer matrix \mathbf{R} , and thus the computational cost. The inertial period and the vertical length scale is still resolved and it is expected that mainly small scale noise is rejected by subsampling the measurements.

The model was initialized by the first measurements collected the 30th of June 1982 and the standard deviation has been set to 0.025 m s^{-1} for both the measurements and the initial condition. The values for the variances and the de-correlation lengths are given in Table 4 while some of the physical parameters used are given in Table 3.

The Ekman model describes wind-driven surface currents and inertial oscillations only, while the measurements may also contain contributions from e.g. pressure-driven currents. Therefore some drift in the measurements has been removed from the deepest moorings as was also done by Yu and O'Brien [1991, 1992].

The results from the inverse calculation is shown in Figures 5 and 6 as time series of the u - and v -component of the velocity at various depths. The inverse estimate is plotted together with the full time series of the measurements. The measurements which were used in the inversion are shown as diamonds.

It is first of all evident that the inverse estimate is close to the measurements at all times and depths, also at 10 m where no measurements were assimilated. Both the amplitude and phase are in good agreement with the measurements at all depths. Note also that the inverse estimate is smooth and it does not interpolate the measurements, however, it is close to the measurements at all depths. By a closer examination of the inverse estimate, it is possible to see that the time derivative of the inverse estimate is discontinuous at measurement locations. This is caused by neglecting the time correlation in the model error covariances.

The posterior error variances $\mathbf{C}_{uu}(z, t, z, t)$ are given

by equation (32), and normally the prior error variances $\mathbf{F}(z, t, z, t)$ are calculated from a statistical simulation, [see e.g. Evensen, 1994b]. However, note that from equations (30) and (33),

$$\mathbf{R} = \mathcal{L}\mathcal{L}^T[\mathbf{F}]. \quad (43)$$

The use of direct measurements implies that the diagonal of the representer matrix \mathbf{R} will contain the error variances at the measurement locations. Having a high density of measurements and assuming a smooth prior error variance field in space and time makes it possible to interpolate the prior error variances at measurement locations to the full space-time grid. Thus, the posterior error variances are readily calculated without much computational effort.

In Figure 11, the prior and posterior error variances for the u -component of the horizontal velocity \mathbf{u} at 5 m and 50 m are shown, respectively. What may be observed, is that the prior errors are growing in time as a result of incorporating model errors. The posterior error variances have the characteristic structure one would expect from a smoother solution for linear dynamics, with minimum values at the measurement locations [see e.g. Bennett and Budgell, 1989]. The error estimates are given for the final iteration in the estimation of the diffusion A and the wind drag C_d , and are thus those corresponding to the best estimates of the parameters.

The results of the estimation of the vertical diffusion parameter are shown in Figure 7. It generally decreases at all depths from the first guess profile, e.g. at the surface from the first guess value 0.0003 to $0.00035 \text{ m}^2 \text{ s}^{-1}$. The corresponding value found by Yu and O'Brien [1991] starting from a first guess of $0.00001 \text{ m}^2 \text{ s}^{-1}$, was $0.0029 \text{ m}^2 \text{ s}^{-1}$.

The wind drag coefficient C_d converges rapidly from the first guess value 0.001 to the value 0.00068 as shown in Figure 8. The value found by Yu and O'Brien [1991] was 0.00126 starting from 0.00134 .

There is a substantial difference in the values for the diffusion coefficient and the wind drag obtained in the two works. It should be noted that while they replaced the first guess values, C_{d_0} and $A_0(z)$ with the current estimate in each iteration of the equations (18) and (19), these were kept constant in our calculations. Clearly, Yu and O'Brien [1991] solved a different inverse problem in each iteration. Actually, it is not clear from their figures that their iterations did converge.

By comparing our results for the diffusion parameter and wind drag coefficient with results found by e.g., Price *et al.* [1987] who inferred an effective viscosity $A = 0.006 \text{ m}^2 \text{ s}^{-1}$ by separating the wind-driven current from the measured LOTUS-3 current and averaging over the whole period, it may seem as if our final diffusion and wind drag are too small. The reason for still getting good results for the inverse estimate may be that the measurements are compensating for the low vertical mixing through the assimilation process.

For comparison a strong constraint inversion was performed and the results are shown in Figures 9 and 10. The final estimates of the diffusion A and the wind drag C_d from the weak constraint inversion were used. Note, that the strong constraint inverse for a linear model is easily solved for without any iterations simply by calculating the representer solution with the model error covariance set to zero.

It is clear from comparisons, that the strong constraint solution in the upper part of the ocean is in reasonable phase with the measurements, as determined by the initial conditions, while the amplitudes are not as good as in the weak constraint inverse. The only way the amplitudes can change when the model is assumed to be perfect is by vertical transfer of momentum from the surface. This is seen to work reasonably well near the surface, while in the deeper ocean there is hardly any effect from the wind stress, and the strong constraint inverse solution is also far from the measurements. The solution is actually rather close to a sine curve representing the pure inertial oscillations. The strong constraint results from *Yu and O'Brien* [1992] are similar to ours and also have the same problems with amplitude and phase.

These results indicate that model deficiencies, such as neglected physics, should be accounted for through a weak constraint variational formulation to ensure an inverse solution in agreement with the measurements.

Summary

A combined parameter estimation and weak constraint inverse problem has been formulated for a one-dimensional Ekman model. The formulation of the inverse problem and the solution method which is based on the representer method has been outlined and discussed in some detail. The inclusion of unknown physical parameters as control variables yields a nonlinear inverse problem even if the model itself is linear. It has been illustrated how an iterative technique in combination with the representer method can be used to estimate poorly known parameters in the model. This was done by defining an iteration for the unknown parameters in the Euler–Lagrange equations, and then solving each linear iterate exactly using the representer method. In addition to illustrating the method on a simple twin experiment, a comparison was also made with the strong constraint solution found by *Yu and O'Brien* [1991, 1992], where measurements from the LOTUS-3 data set were assimilated. It was shown that the weak constraint inverse solution was in good agreement with the observations and that it was superior to the strong constraint inverse.

Acknowledgments Mette Eknes was supported by a grant from the Nansen Environmental and Remote Sensing Center and Geir Evensen was supported by the Norwegian Research Council.

References

- Bennett, A. F., *Inverse Methods in Physical Oceanography*, Cambridge University Press, 1992.
- Bennett, A. F., and J. R. Baugh, A parallel algorithm for variational assimilation in oceanography and meteorology, *J. Atmos. Ocean. Tech.*, **9**, 426–433, 1992.
- Bennett, A. F., and W. P. Budgell, The Kalman smoother for a linear quasigeostrophic model of ocean circulation, *Dyn. Atmos. Oceans*, **13**(3-4), 219–267, 1989.
- Bennett, A. F., L. M. Leslie, C. R. Hagelberg, and P. E. Powers, Tropical cyclone prediction using a barotropic model initialized by a generalized inverse method, *Mon. Weather Rev.*, **121**, 1714–1729, 1993.
- Bennett, A. F., and R. N. Miller, Weighting initial conditions in variational assimilation schemes, *Mon. Weather Rev.*, **119**, 1098–1102, 1990.
- Bennett, A. F., and M. Thorburn, The generalized inverse of a nonlinear quasigeostrophic ocean circulation model, *J. Phys. Oceanogr.*, **22**, 213–230, 1992.
- Bowers, C. M., J. F. Price, R. A. Weller, and M. G. Briscoe, Data tabulations and analysis of diurnal sea surface temperature variability observed at LOTUS, Tech. Rep. 5, Woods Hole Oceanographic Institution (WHOI), 1986.
- Evensen, G., Inverse methods and data assimilation in nonlinear ocean models, *Physica D*, **77**, 108–129, 1994a.
- Evensen, G., Sequential data assimilation with a nonlinear quasi-geostrophic model using Monte Carlo methods to forecast error statistics, *J. Geophys. Res.*, **99**(C5), 10,143–10,162, 1994b.
- Price, J. F., R. A. Weller, and R. Schudlich, Wind-driven ocean currents and Ekman transport, *Science*, **238**, 1534–1538, 1987.
- Smedstad, O. M., and J. J. O'Brien, Variational data assimilation and parameter estimation in an equatorial Pacific Ocean model, *Prog. Oceanog.*, **26**, 179–241, 1991.
- Tarbell, S. A., N. J. Pennington, and M. G. Briscoe, A compilation of moored current meter and wind recorder data: Long-term upper ocean study (LOTUS), May 1982–April 1983., Tech. Rep. 36, Woods Hole Oceanographic Institution (WHOI), 1984.
- Yu, L., and J. J. O'Brien, Variational estimation of the wind stress drag coefficient and the oceanic eddy viscosity profile, *J. Phys. Oceanogr.*, **21**, 709–719, 1991.

List of Tables

1	Physical parameters used in the twin experiment.	11
2	Dimensional values of the variances and the de-correlation lengths used in the twin experiment.	11
3	Physical parameters used in the LOTUS-3 data assimilation experiment.	11
4	Dimensional values for the variances and the de-correlation lengths used in the LOTUS-3 data assimilation experiment.	12

List of Figures

1	Solution from the identical twin experiment. The left and right column contains respectively the u - and v -components of the first guess estimate \mathbf{u}_F (top), the reference case \mathbf{u} (second row), the inverse estimate $\hat{\mathbf{u}}$ (third row), and the error variance reduction (bottom). The contour intervals are 0.05 m s^{-1} for the velocity plots and $0.00006 \text{ m}^2 \text{ s}^{-2}$ for the error variance reduction.	13
2	The u - and v -components (left and right column, respectively) of α_5 (top), $\mathbf{Q}_{qq} \bullet \alpha_5$ (second row), \mathbf{r}_5 (third row), the adjoint λ (fourth row), and $\mathbf{Q}_{qq} \bullet \lambda$ (bottom), from the identical twin experiment. The measurement locations are marked with an asterisk.	14
3	The estimation of the eddy viscosity profile A from the identical twin experiment.	15
4	The estimation of the wind drag coefficient C_d from the identical twin experiment. The number of iterations are given along the x -axis.	15
5	Weak constraint inverse estimate (solid line), the time series of measurements (dashed lines), and the subsampled measurements (diamonds) at 5 m, 10 m and 25 m from the LOTUS-3 data assimilation experiment. The u - and v -components are shown in the left and right column, respectively.	16
6	Same as Figure 5 but for the depths 35 m, 50 m and 75 m.	17
7	Results of the estimation of the eddy viscosity profile A from the LOTUS-3 data assimilation experiment.	18
8	Results of the estimation of the wind drag C_d from the LOTUS-3 data assimilation experiment.	18

9	Strong constraint inverse estimate (solid line), the time series of measurements (dashed lines), and the subsampled measurements (diamonds) at 5 m, 10 m and 25 m from the LOTUS-3 assimilation experiment. The u - and v -components are shown in the left and right column, respectively.	19
10	Same as Figure 9 but for the depths 35 m, 50 m and 75 m.	20
11	The error variance for the u -component of the inverse estimate at 5 m (to the left) and 50 m (to the right) in the weak constraint case.	21

Table 1. Physical parameters used in the twin experiment.

Symbol	Description	Value
T	Integration time	50 hours
Δt	Time step	6 minutes
H	Depth	40 m
Δz	Grid size	1.4 m
f	Coriolis parameter	$1.3 \times 10^{-6} \text{ s}^{-1}$
δ_E	Ekman layer thickness	6.3 m
ρ_a	Density of air	1.2 kg m^{-3}
ρ_w	Density of water	$1.025 \times 10^3 \text{ kg m}^{-3}$

Table 2. Dimensional values of the variances and the de-correlation lengths used in the twin experiment.

Symbol	Description	Value
σ_q^2	Model error variance	$1.0 \times 10^{-13} \text{ m}^2 \text{ s}^{-4}$
σ_a^2	Initial error variance	$0.0025 \text{ m}^2 \text{ s}^{-2}$
$\sigma_{b_0}^2$	Boundary error variance	$3.0 \times 10^{-10} \text{ m}^4 \text{ s}^{-4}$
$\sigma_{b_H}^2$	Boundary error variance	$3.0 \times 10^{-10} \text{ m}^4 \text{ s}^{-4}$
σ_o^2	Measurement error variance	$2.5 \times 10^{-5} \text{ m}^2 \text{ s}^{-2}$
σ_A^2	Diffusion error variance	$6.25 \times 10^{-8} \text{ m}^4 \text{ s}^{-2}$
$\sigma_{C_d}^2$	Wind drag error variance	1.7×10^{-8}
l_q	e-folding scale for model error covariance	$1.0 \delta_e$
l_a	e-folding scale for initial error covariance	$1.0 \delta_e$
l_A	e-folding scale for diffusion error covariance	$2.0 \delta_e$

Table 3. Physical parameters used in the LOTUS-3 data assimilation experiment.

Symbol	Description	Value
T	Integration time	240 hours
Δt	Time step	30 minutes
H	Depth	100 m
Δz	Grid size	0.5 m
f	Coriolis parameter	$0.8 \times 10^{-4} \text{ s}^{-1}$
δ_E	Ekman layer thickness	2.71 m
ρ_a	Density of air	1.2 kg m^{-3}
ρ_w	Density of water	$1.025 \times 10^3 \text{ kg m}^{-3}$

Table 4. Dimensional values for the variances and the de-correlation lengths used in the LOTUS-3 data assimilation experiment.

Symbol	Description	Value
σ^2	Model error variance	$5.0 \times 10^{-12} \text{ m}^2 \text{ s}^{-4}$
σ_a^2	Initial error variance	$6.25 \times 10^{-4} \text{ m}^2 \text{ s}^{-2}$
$\sigma_{b_0}^2$	Boundary error variance	$3.0 \times 10^{-10} \text{ m}^4 \text{ s}^{-4}$
$\sigma_{b_H}^2$	Boundary error variance	$3.0 \times 10^{-10} \text{ m}^4 \text{ s}^{-4}$
σ_o^2	Measurement error variance	$6.25 \times 10^{-4} \text{ m}^2 \text{ s}^{-2}$
σ_A^2	Diffusion error variance	$0.5 \times 10^{-8} \text{ m}^4 \text{ s}^{-2}$
$\sigma_{C_d}^2$	Wind drag error variance	1.7×10^{-8}
l_q	e -folding scale for model error covariance	$2.2\delta_e$
l_a	e -folding scale for initial error covariance	$2.2\delta_e$
l_A	e -folding scale for diffusion error covariance	$5.0\delta_e$

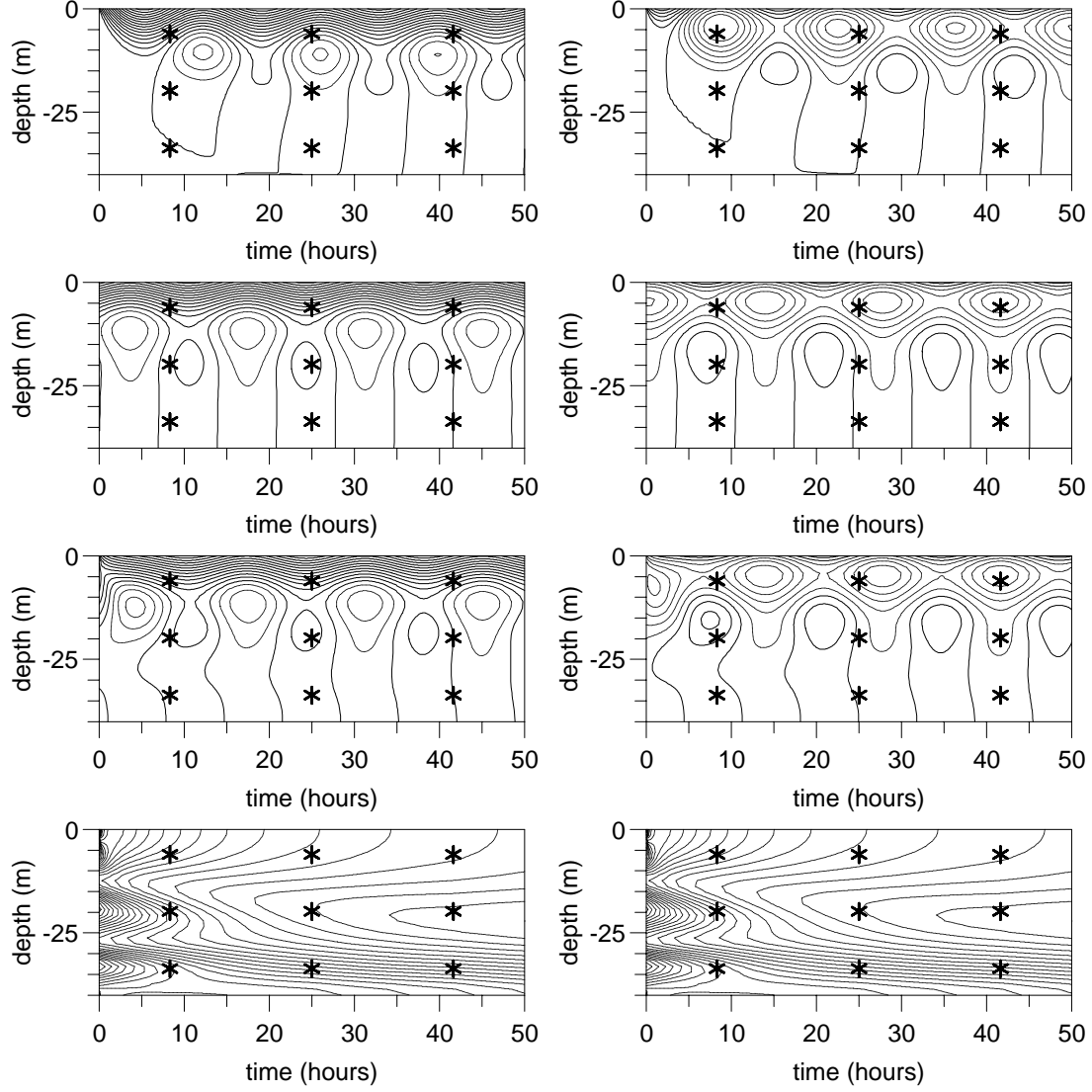


Figure 1. Solution from the identical twin experiment. The left and right column contains respectively the u - and v -components of the first guess estimate \mathbf{u}_F (top), the reference case \mathbf{u} (second row), the inverse estimate $\hat{\mathbf{u}}$ (third row), and the error variance reduction (bottom). The contour intervals are 0.05 m s^{-1} for the velocity plots and $0.00006 \text{ m}^2 \text{ s}^{-2}$ for the error variance reduction.

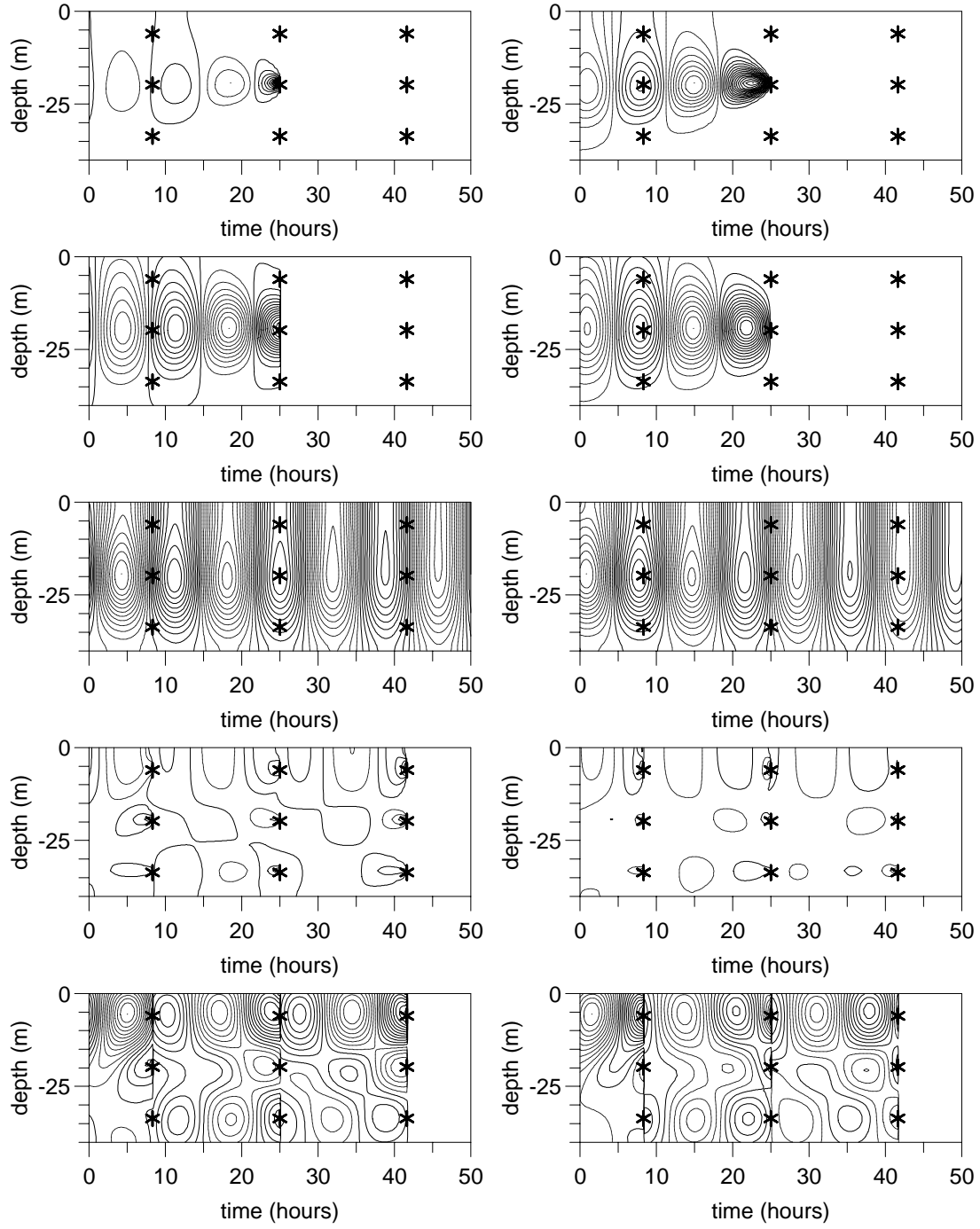


Figure 2. The u - and v -components (left and right column, respectively) of α_5 (top), $Q_{qq} \bullet \alpha_5$ (second row), r_5 (third row), the adjoint λ (fourth row), and $Q_{qq} \bullet \lambda$ (bottom), from the identical twin experiment. The measurement locations are marked with an asterisk.

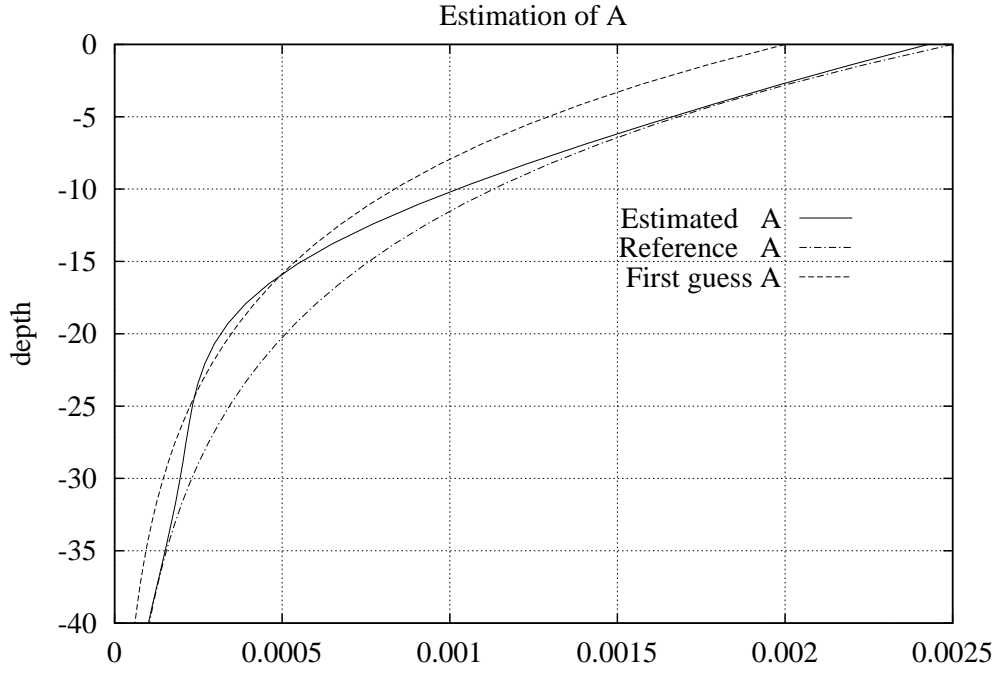


Figure 3. The estimation of the eddy viscosity profile A from the identical twin experiment.

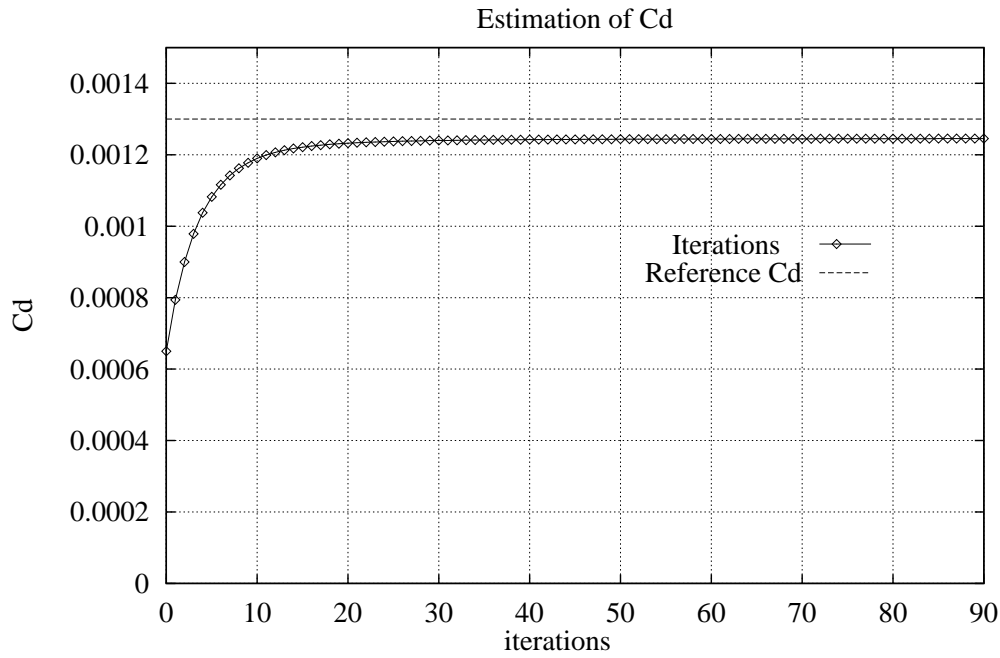


Figure 4. The estimation of the wind drag coefficient C_d from the identical twin experiment. The number of iterations are given along the x -axis.

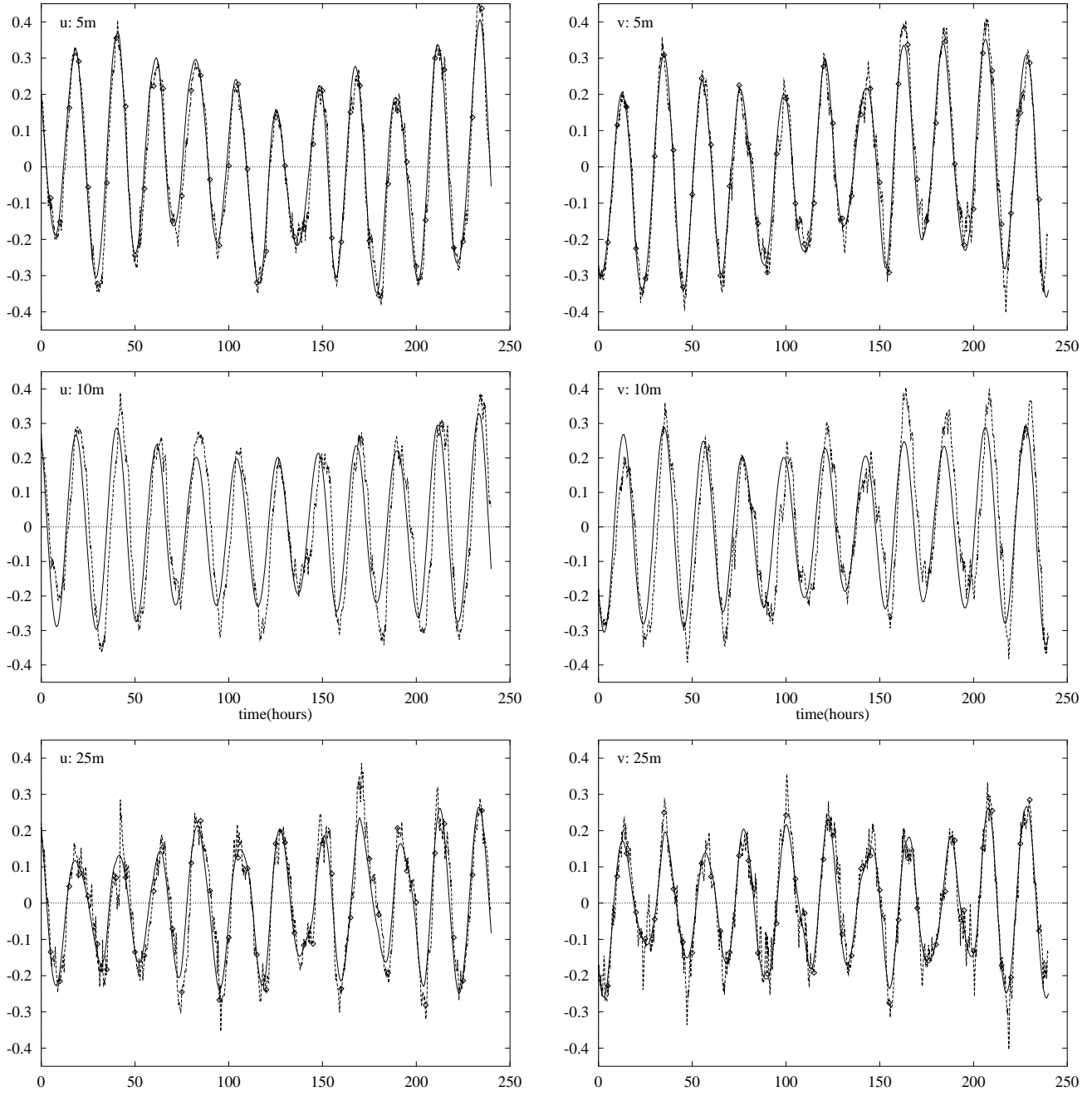


Figure 5. Weak constraint inverse estimate (solid line), the time series of measurements (dashed lines), and the subsampled measurements (diamonds) at 5 m, 10 m and 25 m from the LOTUS-3 data assimilation experiment. The u - and v -components are shown in the left and right column, respectively.

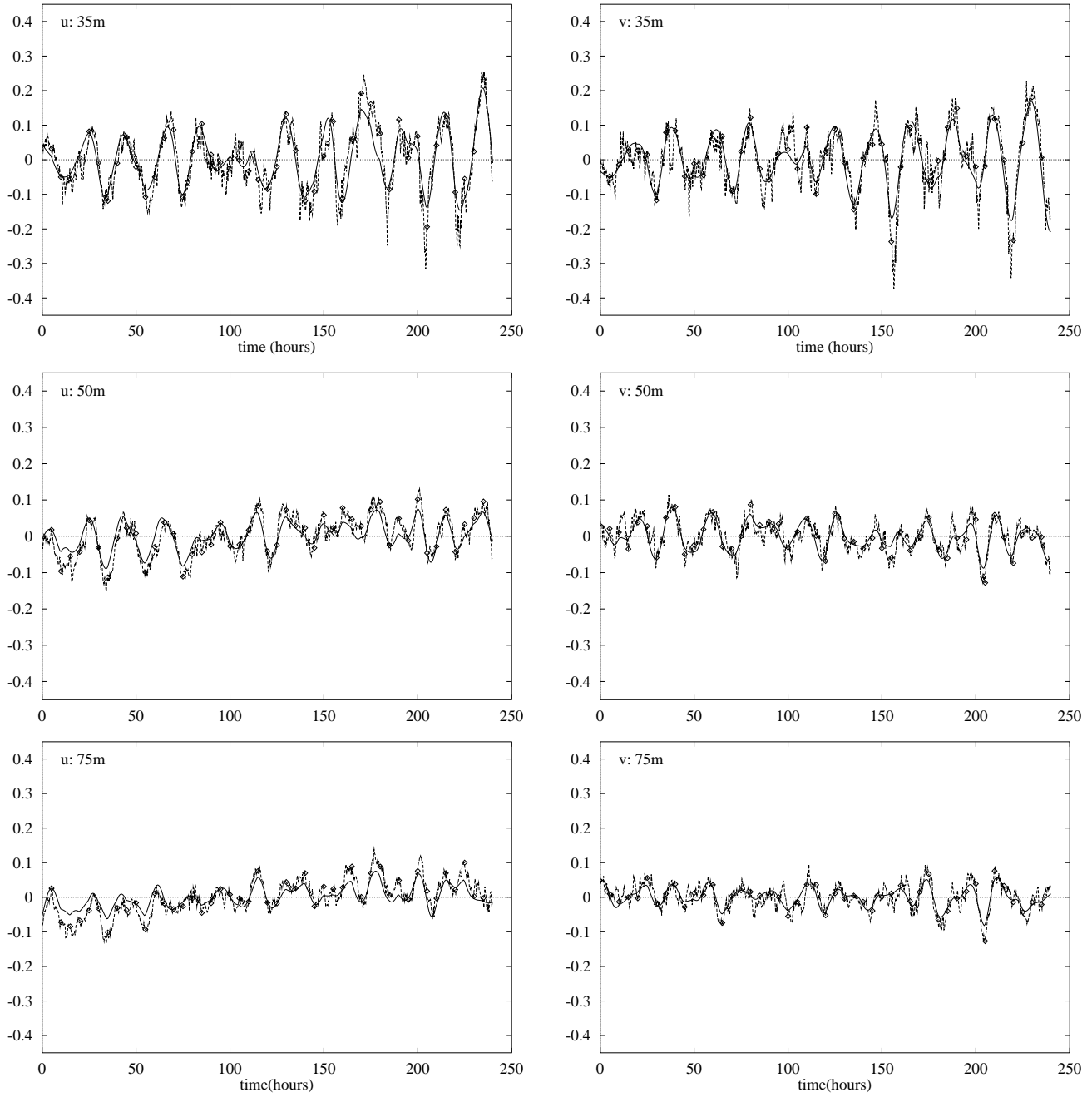


Figure 6. Same as Figure 5 but for the depths 35 m, 50 m and 75 m.

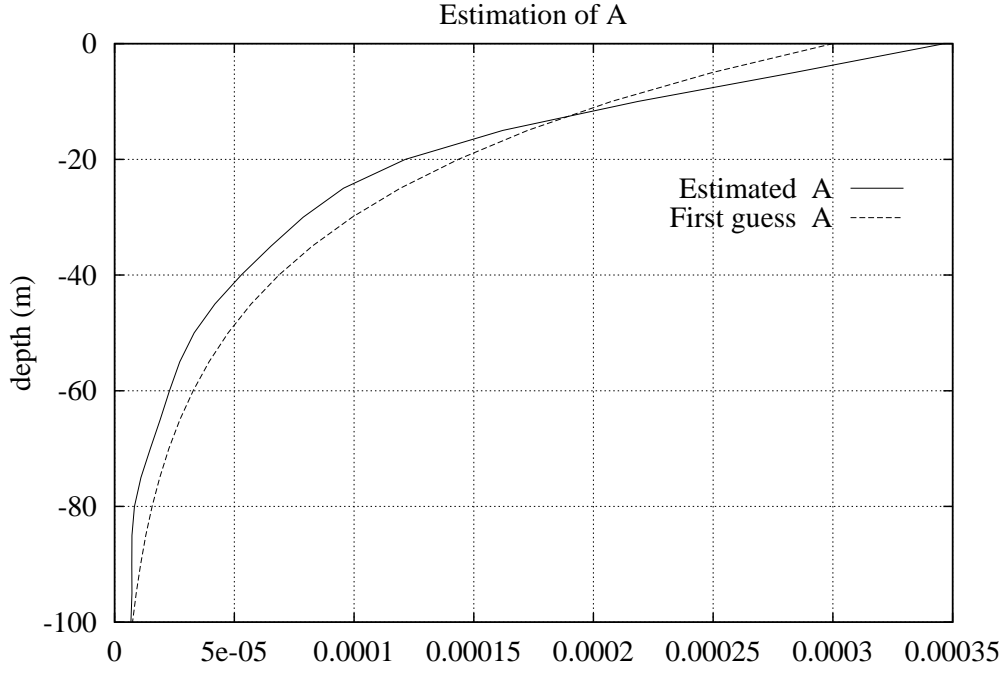


Figure 7. Results of the estimation of the eddy viscosity profile A from the LOTUS-3 data assimilation experiment.

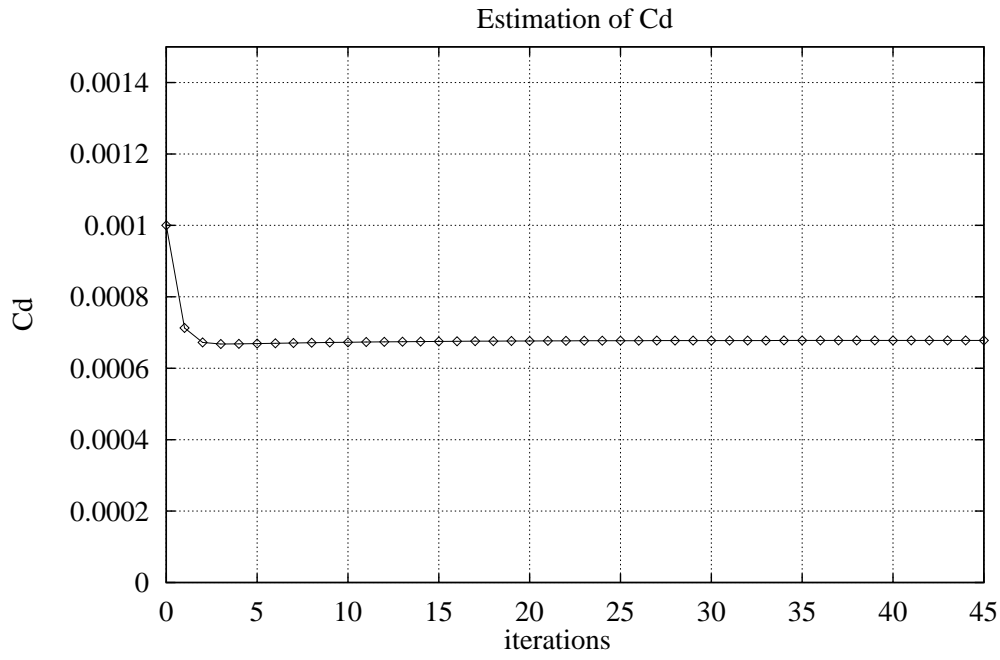


Figure 8. Results of the estimation of the wind drag C_d from the LOTUS-3 data assimilation experiment.

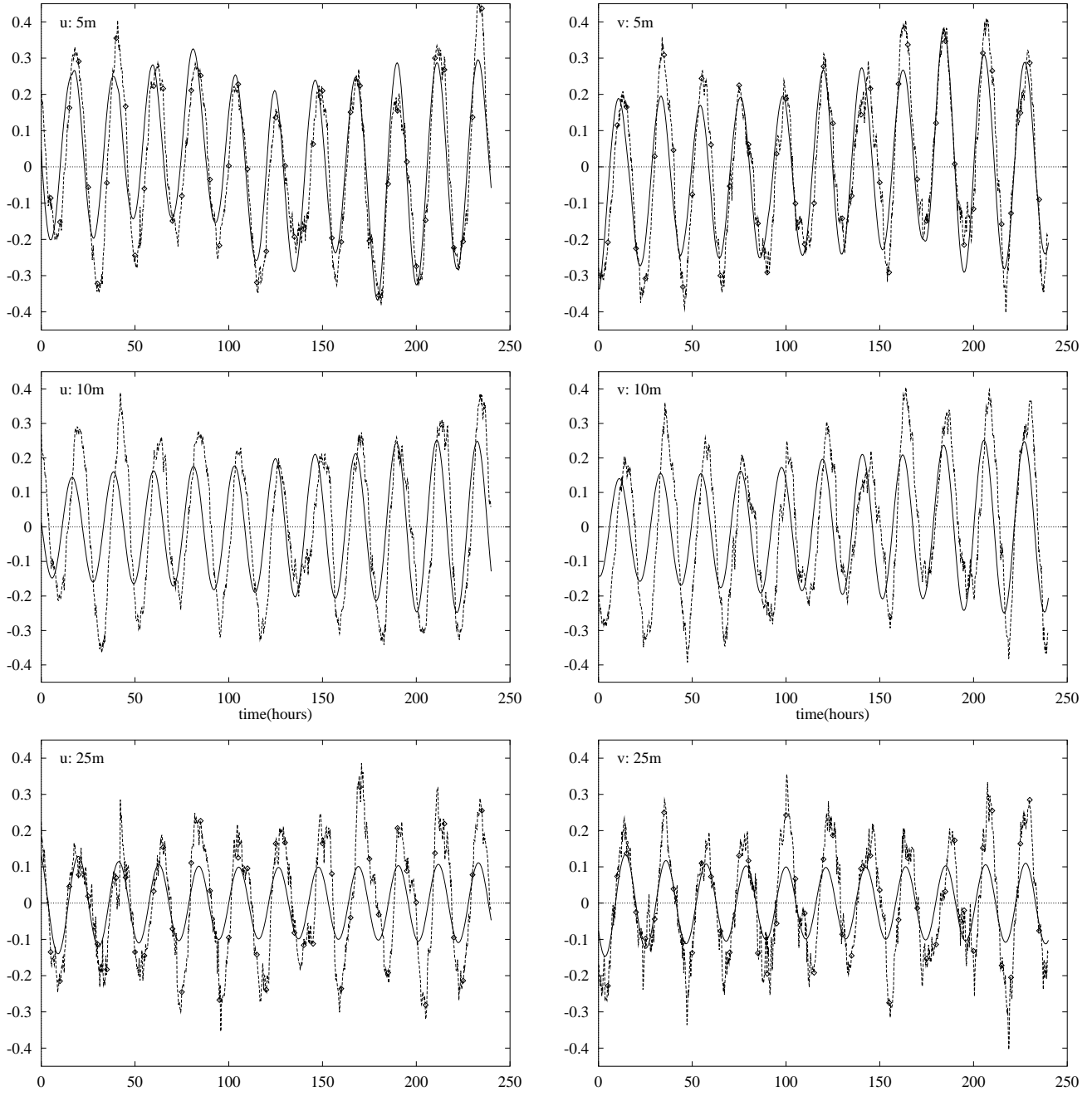


Figure 9. Strong constraint inverse estimate (solid line), the time series of measurements (dashed lines), and the subsampled measurements (diamonds) at 5 m, 10 m and 25 m from the LOTUS-3 assimilation experiment. The u - and v -components are shown in the left and right column, respectively.

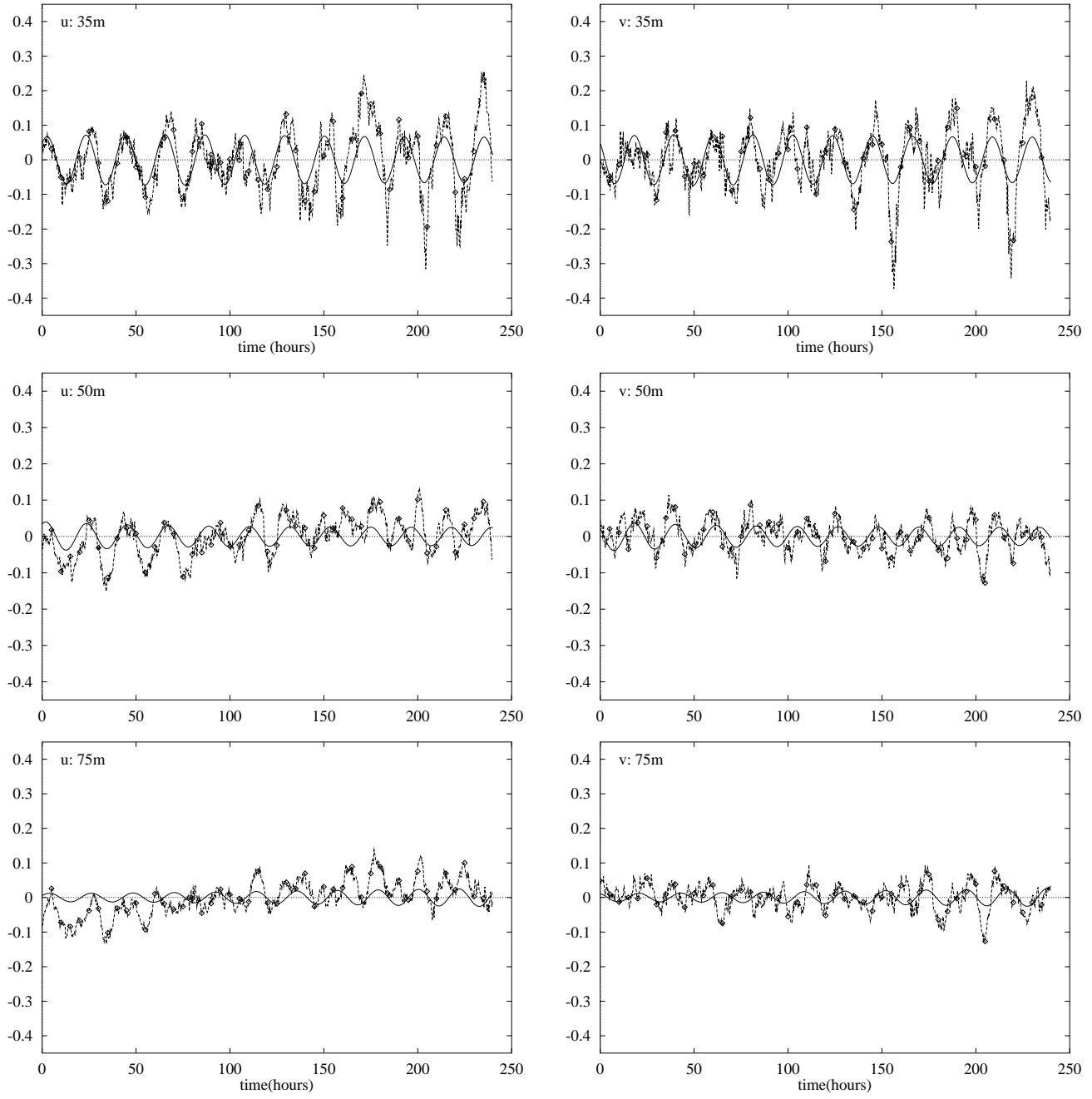


Figure 10. Same as Figure 9 but for the depths 35 m, 50 m and 75 m.

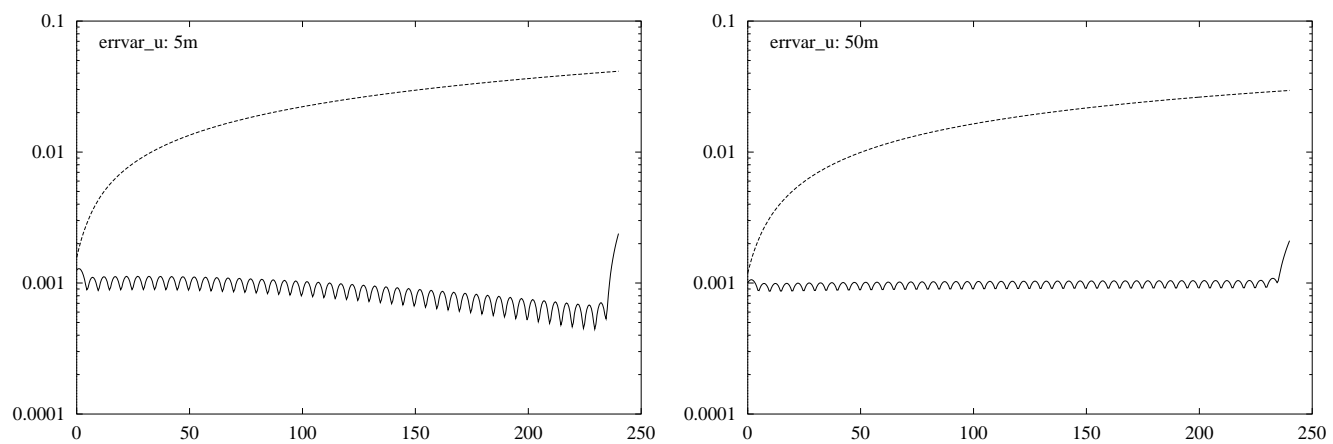


Figure 11. The error variance for the u -component of the inverse estimate at 5 m (to the left) and 50 m (to the right) in the weak constraint case.